Positioning the Adjacent Buried Objects Using UWB Technology Combine with Levenberg-Marquardt Algorithm

Huyen NGUYEN [1], *Ha DUONG* [1], *Hiep PHAM* [2]

[1]Theory Circuits and Measurement, Faculty of Radio Electronic Engineering,
Le Quy Don Technical University, 236 Hoang Quoc Viet, Ha Noi, Vietnam
[2]Wireless Technology, Faculty of Radio Electronic Engineering,
Le Quy Don Technical University, 236 Hoang Quoc Viet, Ha Noi, Vietnam

nguyenhuyen@mta.edu.vn, duongha@mta.edu.vn, phamthanhhiep@gmail.com

DOI: 10.15598/aeee.v20i1.4355

Article history: Received Sep 07, 2021; Revised Dec 04, 2021; Accepted Feb 04, 2022; Published Mar 31, 2022.

Abstract. *The determination of the buried objects and cracks in building structures is an important issue in real-life. In this paper, we propose a new method called Correlation Function Separation Technique (CFST) combine with the Lervenberg-Marquardt Algorithm (LMA) using the Impulse Radio Ultra-Wide Band (IR-UWB) penetrating system to improve the accuracy in detecting and positioning of the adjacent buried objects in building structures. Based on the UWB signal processing, the proposed method can be used to determine both the relative permittivity of the environment and the position of the buried objects, especially the adjacent objects. The analytical method is validated by mathematical proofs and Matlab simulations, and the position errors are used to assess the performance of proposed method. The numerical results shown that the proposed method can be used for positioning the adjacent buried objects in the homogeneous environment which has an average positioning error of* 3.52 *cm, which is smaller than that of the conventional method based on B-canned radar images processing.*

Keywords

Detecting buried object, IR-UWB, Levenberg-Marquardt algorithm, TOA estimation.

1. Introduction

Recently, methods to determine the position of objects in Non-Light-Of-Sight (NLOS) transmission environments have attracted a lot of researches and achieved significant results in Internet of Things (IoT) networks, indoor positioning systems, hospital monitoring and surveillance systems, radar penetration, etc.

A number of signal analysis techniques and system models are proposed for distance measurement and object positioning such as Radio Frequency Identification in IoT network applications [1], using UWB technology combined with median and Kalman filters [2] in free space. In the underground environment, building structures, various techniques used for locating the underground pipelines such as Ground Penetrating Radar (GPR) [3] and [4]. The detection of buried objects in shallow sea with large bandwidth and low frequency electromagnetic waves proposed in [5] can overcome the limitations of acoustic waves and blue-green lasers.

From the above research results, it can be seen that the resolution and detection distance of these non-destructive techniques strongly depend on the signal shapes, the system bandwidth and the material of the buried objects (plastic or metal) as well as information of environmental properties (relative permittivity).

The GPR devices can provide a high image resolution and efficient data processing when using amplitude modulated signals [6], wide-band chaotic signals based on time domain correlation and back-projection algorithm [7], or combines GPR and the electric field method in detecting the depth and radius of plastic pipe [8], using fast and sophisticated reconstruction technique to create the 2D image of the buried target for GPR systems [9]. However in these techniques, the images of underground objects heavily depends on the propagation velocity in signal processing, hence the determination of the relative permittivity of the environment is necessary, but the relative permittivity cannot be determined by image processing.

Using the acoustic signal, it is possible to locate buried objects even when the transmission medium is wet, but this method is strongly influenced by noise [10] and also impossible to determine the wave velocity. Moreover, when the distance between the buried objects is very small, the methods based on GPR, machine learning and acoustic signals are indistinguishable. Therefore, the use of ultra-wide band radio impulses to increase discrimination of identifying adjacent buried objects is a good solution. The very large bandwidth and high spatial resolution makes IR-UWB signal attractive for penetration applications [11] and [12] and became one of the good candidates for positioning techniques especially in the building structures [13] and [14].

In order to increase the ability to distinguish adjacent buried objects and hence, improve the positioning errors, we propose the method of correlation function separation, called CFST combine with the Lervenberg-Marquardt Algorithm (LMA) [15] which is used to process the reflected UWB signal from the buried objects. The method can be used to determine the relative permittivity of the environment, and the positions of the buried objects for both homogeneous and heterogeneous environments. The contributions of the paper are summarized as follows:

- Constructing a system model for positioning a single buried object in a homogeneous medium, and determining the position of the object and the relative permittivity of environment by using the LMA.

- A new positioning algorithm for adjacent buried objects in the homogeneous environment is proposed, named CFST.

The rest of the paper is organized as follows. Section 2. presents the positioning of buried object system model. Mathematical analysis of the correlation functions for the cases of single and adjacent buried objects and LMA are presented in Subsec. 2.2. and Subsec. 2.3. Numerical results are presented in Sec. 3. Finally, Sec. 4. concludes the work.

2. Proposal of Positioning Algorithm

2.1. System Model

The model of a UWB penetrating system is illustrated in Fig. 1, the transmission medium has a relative permittivity of ε, receiver and transmitter antennas are placed in the same position with an assumption of height of 0 m to the environment's surface. The transmitted signal is UWB radio pulse and denoted as $s(t)$, the reflected signal is denoted as $r(t)$, which is a sum of the reflected signals from the buried objects. To determine the propagation distance, on the receiver side, $r(t)$ is correlated with the template signal, then the delay time between the transmitted and reflected signals is computed. The delay time in this paper is called as the traveling time. The parameters of the model are described as follows:

- The transmitted IR-UWB signal takes the form [16]:

$$s(t) = \sqrt{P} \sum_{i=0}^{N} p(t - iT), \tag{1}$$

where P is the transmit power, N is the number of transmitted pulses, T is the repetitive period of the pulse and $p(t)$ is the signal pulse for IR-UWB systems, including Gaussian monocycles, Manchester monocycle and modified Hermite pulse [17].

- The reflected signal is described as:

$$r(t) = \sum_{i=0}^{M} \left[A_i s(t - \tau_i) + n_i(t) \right], \tag{2}$$

where M is the number of buried objects, $\{A_i\}_{i=1}^{M}$ represent the attenuation of the transmission medium and distance, τ_i represents the traveling time of the reflected signals from the i^{th} buried object, and $n_i(t)$ is additive white Gaussian noise.

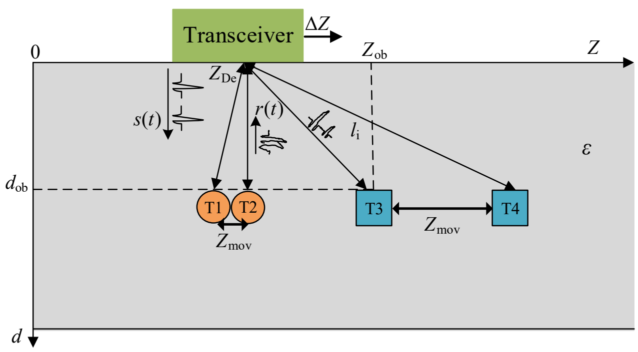

Fig. 1: The model of a UWB penetrating system.

- The template signal at the receiver is $p(t)$, and the correlation function at the receiver side is determined by:

$$R(\delta) = \int_{-\infty}^{\infty} r(t)p(t-\delta)dt. \tag{3}$$

- The traveling time is calculated as:

$$\begin{aligned}\tau_i &= \operatorname{Arg}\max_{\delta}\{R(\delta)\} = \\ &= \operatorname{Arg}\max_{\delta}\left\{\int_{-\infty}^{\infty} r(t)p(t-\delta)dt\right\}.\end{aligned} \tag{4}$$

- The propagation velocity in the system is [18]:

$$V = \frac{c}{\sqrt{\varepsilon}}, \tag{5}$$

  where $c = 3 \cdot 10^8$ m·s^{-1} is the velocity of light in the vacuum environment.

- The distance from the device to the i^{th} buried object with assumption that the transmission medium is homogeneous:

$$l_i = \frac{1}{2}V\tau_i. \tag{6}$$

In this model, we consider two cases, in the first case, two buried objects are assumed to be very close to each other (T1, T2), in which, the reflected signals from two buried objects overlap. In the other case, two buried objects are far away from each other (T3, T4), in which, the reflected signals from those objects do not overlap. An example illustrates two types of the reflected signal as shown in Fig. 2.

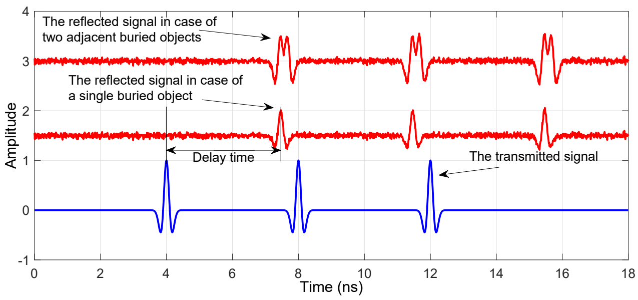

Fig. 2: The transmitted and reflected signals with added noise.

In the UWB systems, the pulse shape has a strong influence on their performance, we first restrict our analysis to the 2^{nd} Gaussian monocycle, the 3^{rd} and 4^{th} oder are investigated in Subsec. 3.2. for comparing and choosing the suitable pulse shape. The 2^{nd} oder Gaussian monocycle given by [17]:

$$\begin{aligned} g_2(t) &= B_{2p}\frac{d^2}{dt^2}e^{-2\pi\left(\frac{t}{T_p}\right)^2} = \\ &= B_{2p}\left[1-4\pi\left(\frac{t}{T_p}\right)^2\right]e^{-2\pi\left(\frac{t}{T_p}\right)^2}, \end{aligned} \tag{7}$$

where T_p represents time normalization factor, the shapes of the auto-correlation functions of the 2^{nd}, 3^{rd} and 4^{th} order Gaussian monocycles are presented in Fig. 3. The performance analysis of the system is considered first with a single buried object, then with adjacent buried objects in the homogeneous environment.

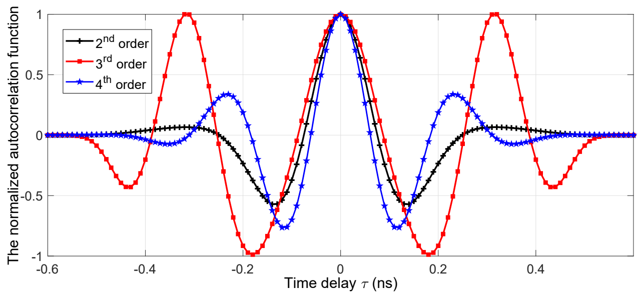

Fig. 3: The auto-correlation function of the Gaussian pulses as a function of time.

2.2. Positioning a Single Buried Object

As seen in Fig. 1, the parameters d_{ob}, Z_{ob} are depth and horizontal coordinates of a single buried object in the 2D space; Z_{Dei}, ΔZ, and l_i are horizontal position, the movement step of the device and distance from the object to device at its i^{th} position, respectively. These parameters are determined as follows:

$$Z_{\text{Dei}} = i \cdot \Delta Z, \quad l_i = \sqrt{(Z_{\text{ob}} - Z_{\text{Dei}})^2 + d_{\text{ob}}^2}. \tag{8}$$

The traveling time is given by:

$$\begin{aligned}\tau_i &= 2\frac{\sqrt{\varepsilon\left[(Z_{\text{ob}} - Z_{\text{Dei}})^2 + d_{\text{ob}}^2\right]}}{c} = \\ &= 2\frac{\sqrt{\varepsilon\left[(Z_{\text{ob}} - i\cdot\Delta Z)^2 + d_{\text{ob}}^2\right]}}{c},\end{aligned} \tag{9}$$

τ_i is calculated according to Eq. (4). In Eq. (9), the values of τ_i, i, and Z_{Dei} are known, and the values of ε, Z_{ob}, and d_{ob} are estimated by the LMA so that the cost function reaches the minimum value. Accordingly, those parameters are considered as the coefficients of the nonlinear equations. Their values are determined based on a given set of pair (Z_{Dei}, τ_i), and the cost function is given in Eq. (11).

The unknown parameter vector is denoted by:

$$\vec{X} = (\varepsilon, Z_{\text{ob}}, d_{\text{ob}}) . \tag{10}$$

The estimated value $\widehat{\vec{X}}$ of $\vec{X}$ is determined such that:

$$\begin{aligned} \widehat{\vec{X}} &= \operatorname{Arg} \min_{\widehat{\vec{X}}} S\left(\widehat{\vec{X}}\right) = \\ &= \operatorname{Arg} \min_{\widehat{\vec{X}}} \sum_{i=1}^{K} \left[\tau_i - f\left(Z_{\text{De}i}, \widehat{\vec{X}}\right)\right]^2, \end{aligned} \tag{11}$$

where K is the number of elements in the vector $\vec{Z}_{\text{De}}$ and $f\left(Z_{\text{De}i}, \widehat{\vec{X}}\right)$ has the form:

$$f\left(Z_{\text{De}i}, \widehat{\vec{X}}\right) = 2\frac{\sqrt{\widehat{\varepsilon}\left[\left(\widehat{Z}_{\text{ob}} - Z_{\text{De}i}\right)^2 + \widehat{d}_{\text{ob}}^2\right]}}{c}. \tag{12}$$

The vector $\widehat{\vec{X}}$ is determined by the following steps and shown in flowchart in Fig. 4.

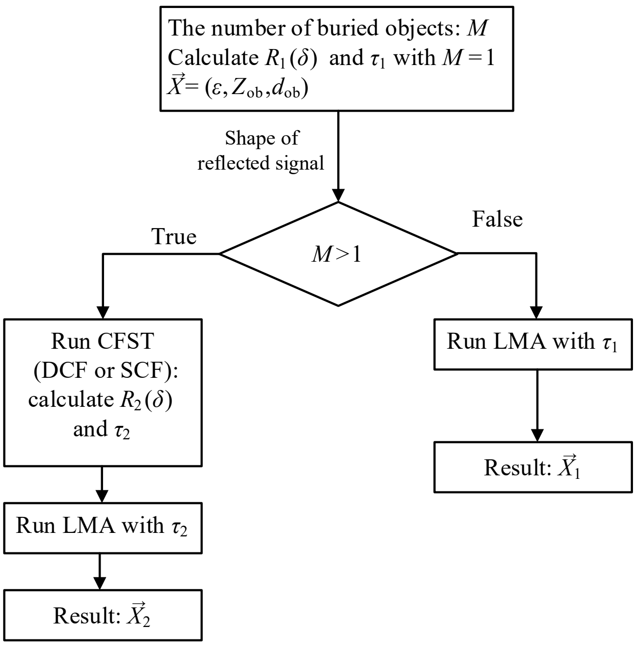

Fig. 4: The flowchart of LMA.

Step 1: $\widehat{\vec{X}}$ is initialized as an arbitrary value $\widehat{\vec{X}}_{\text{int}}$; check the constraint condition in Eq. (11), if it is false, perform step 2, else, stop the algorithm.

Step 2: $\widehat{\vec{X}}_{\text{int}}$ is replaced by the new one $\left(\widehat{\vec{X}} + \vec{\theta}\right)$, with $\vec{\theta}$ being an updated step vector, and calculate the sum:

$$\begin{aligned} \vec{S}(\widehat{\vec{X}} + \vec{\theta}) \approx &\left[\vec{\tau} - \vec{f}\left(\vec{Z}_{\text{De}}, \vec{X}\right)\right]^T \left[\vec{\tau} - \vec{f}\left(\vec{Z}_{\text{De}}, \vec{X}\right)\right] \\ &-2\left[\vec{\tau} - \vec{f}\left(\vec{Z}_{\text{De}}, \vec{X}\right)\right]^T \mathbf{J}\vec{\theta} + \vec{\theta}^T \mathbf{J}^T \mathbf{J}\vec{\theta}, \end{aligned} \tag{13}$$

where $\mathbf{J}$ is the Jacobian matrix, whose i^{th} row equals $\vec{J}_i$ and $\vec{f}\left(\vec{Z}_{\text{De}}, \vec{X}\right)$, $\vec{\tau}$ are vectors of i^{th} component $f\left(Z_{\text{De}i}, \vec{X}\right)$ and τ_i respectively, we have:

$$\vec{J}_i = \frac{\partial f\left(Z_{\text{De}i}, \widehat{\vec{X}}\right)}{\partial \widehat{\vec{X}}}. \tag{14}$$

The sum $\vec{S}\left(\widehat{\vec{X}} + \vec{\theta}\right)$ has its minimum at zero gradient with respect to $\vec{\theta}$, hence $\vec{\theta}$ can be determined satisfying:

$$\left[\mathbf{J}^T\mathbf{J} + \lambda \operatorname{diag}\left(\mathbf{J}^T\mathbf{J}\right)\right]\vec{\theta} = \mathbf{J}^T\left[\vec{\tau} - \vec{f}\left(\vec{Z}_{\text{De}}, \widehat{\vec{X}}\right)\right], \tag{15}$$

where the damping factor λ (non-negative) is adjusted at each iteration. If $\vec{S}$ is reduced rapidly, a smaller value of λ can be used, whereas if $\vec{S}$ does not reduce, λ can be increased.

Step 3: The updated step vector is computed as follows:

$$\vec{\theta} = \left[\mathbf{J}^T\mathbf{J} + \lambda \operatorname{diag}\left(\mathbf{J}^T\mathbf{J}\right)\right]^{-1}\mathbf{J}^T\left[\vec{\tau} - \vec{f}\left(\vec{Z}_{\text{De}}, \widehat{\vec{X}}\right)\right]. \tag{16}$$

The algorithm repeats steps 2 and 3 until the constraint condition in Eq. (11) is satisfied. And the outputs of LMA are the final estimated values of system parameters $\widehat{\vec{X}} = \left(\widehat{\varepsilon}, \widehat{Z}_{\text{ob}}, \widehat{d}_{\text{ob}}\right)$.

2.3. Positioning the Adjacent Buried Objects

Considering the system model in Fig. 1 with two buried objects, the received signal is the sum of the reflected signals from these objects, and are denoted by $r_1(t)$ and $r_2(t)$. In case, the buried objects are very far from each other, such as T3 and T4 in Fig. 1, the reflected signals $r_1(t)$ and $r_2(t)$ do not overlap, consequently we have applied the procedure to locate single object as presented in Subsec. 2.2. . However, in case, the buried objects are near each other, such as T1 and T2 in Fig. 1, the reflected signals $r_1(t)$ and $r_2(t)$ overlap. In this scenario, as shown in Fig. 5, the correlation function shapes are changed with different cases of the buried objects: there is one buried object, two adjacent buried objects and two apart buried objects with Z_{mov} is the distance between the buried objects.

In the case of two apart buried objects, it is entirely possible to apply the method in Subsec. 2.2. to locate one by one buried object. In the case of two adjacent buried objects, the proposed CFST is applied to determine the second object by using the correlation function values and the position of the first object. The

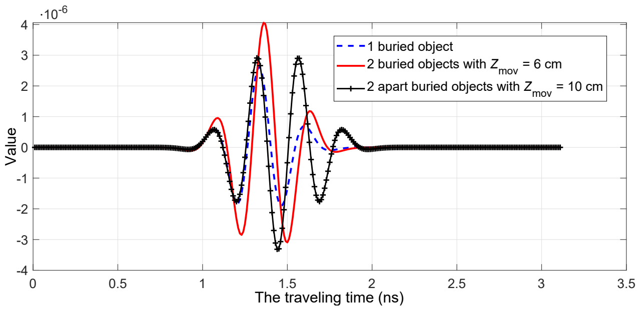

Fig. 5: The correlation function shapes with different distances between buried objects.

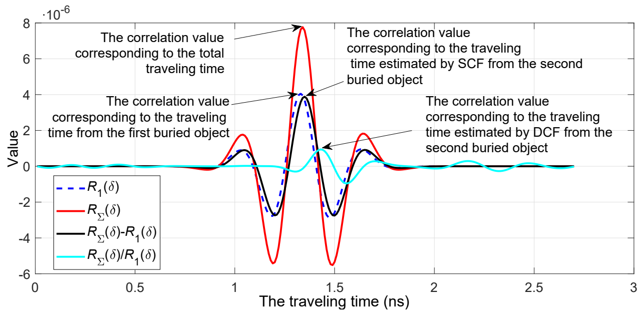

Fig. 6: The correlation function shapes of the reflected signals of conventional and CFST methods when there are two adjacent buried objects (the first object at $(Z_{\mathrm{ob}}, d_{\mathrm{ob}}) =$ (0.3 m, 0.2 m); $Z_{\mathrm{mov1}} = 4$ cm; the transceiver is in $Z_{\mathrm{Dei}} = 0.3$ m).

correlation function has the form:

$$R(\delta) = \int_{-\infty}^{\infty} r_\Sigma(t) p(t-\delta) dt =$$

$$= \int_{-\infty}^{\infty} [r_1(t) + r_2(t)]\, p(t-\delta) dt = R_1(\delta) + R_2(\delta), \tag{17}$$

and the traveling time can be calculated as (Total):

$$\tau_\Sigma = \operatorname{Arg}\max_\delta \{R(\delta)\}. \tag{18}$$

Using the received signal $r_\Sigma(t)$, the traveling time from the second object to the device is denote by τ_2 and can be computed by CFST with two expansions. Firstly, by Subtracting the Correlation Functions (SCF):

$$\tau_2 = \delta_{\mathrm{op}} = \left[\operatorname{Arg}\max_\delta \{R(\delta) - R_1(\delta)\}\right]. \tag{19}$$

Secondly, by Dividing the Correlation Functions (DCF):

$$\tau_2 = \delta_{\mathrm{op}} = \left[\operatorname{Arg}\max_\delta \left\{\frac{R(\delta)}{R_1(\delta)}\right\}\right]. \tag{20}$$

Fig. 6 illustrates the shapes of the correlation functions of reflected signals with the template signal in the case of two adjacent buried objects in the homogeneous environment. The traveling time τ_2 can be estimated according to SCF, DCF and the position of the second object can be located in the same way as presented in the Subsec. 2.2. by using the LMA in which τ is replaced by τ_2. The flowchart of the proposed CFST is illustrated in the Fig. 7.

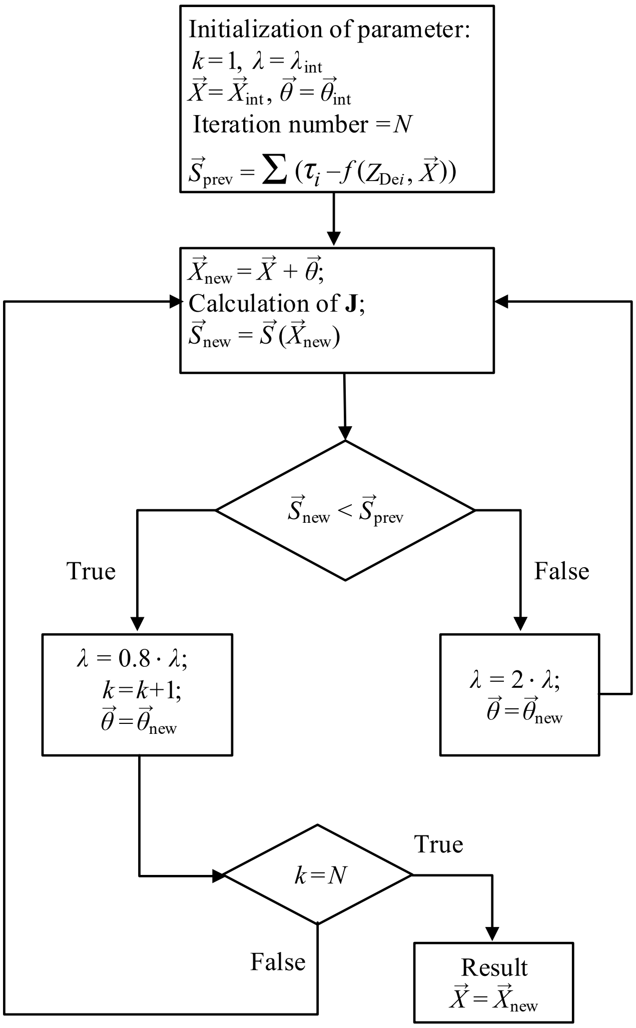

Fig. 7: The flowchart of CSFT.

3. Numerical Results and Comparisons

3.1. System Parameters

An example of the parameters of a penetrating UWB system is listed in Tab. 1. Our above analysis presents that the adjacent buried objects can be located one by one, the position of the following object is determined based on the data set of the correlation function value of the previous object. All the numerical results in this paper were computed using Matlab, the data set of the reflected signals were generated by simulation. Furthermore, the localization technique is based on the Time Of Arrival (TOA), and the Root Mean Squared Error (RMSE) of the CFST is determined by the Eq. (21) and compared with the Cramer-Rao Lower Bound (CRLB) in Eq. (22).

Tab. 1: Simulation parameters [21].

Parameter	Notation	Value
Impulse width	PW	0.7 ns
Transmitted power	P_{Tx}	-5.4 dBm
Noise power	$N_0/2$	-77 dBm
Time normalization factor	T_p	0.2877 ns
Effective bandwidth	ΔF	3.5 GHz
Relative permittivity	ε	4.5
The repetitive period	T	50 ns
Number of pulse	N	100
Movement step of the device	ΔZ	1 cm

The Root Mean Squared Error (RMSE) of the CFST in determining the traveling time τ_2:

$$\mathrm{RMSE} = \sqrt{\frac{1}{N}\sum_{k=1}^{N}\left(\hat{\tau}_{2k}-\tau_2\right)^2}. \tag{21}$$

The CRLB [20] on the standard deviation of an unbiased TOA estimator $\hat{\tau}$ is given by:

$$\sqrt{\mathrm{Var}(\hat{\tau})} \geq \frac{1}{2\sqrt{2}\pi\sqrt{\mathrm{SNR}}\Delta F}, \tag{22}$$

where SNR, ΔF are signal to noise ratio and effective bandwidth, respectively. The change of RMSE vs. SNR for SCF, DCF and Total methods in estimating the traveling time τ_2 are illustrated in Fig. 8 with the case of two adjacent buried objects in the homogeneous environment, the first buried object at a depth of 30 cm, and the second buried object is 4 cm away from the first one.

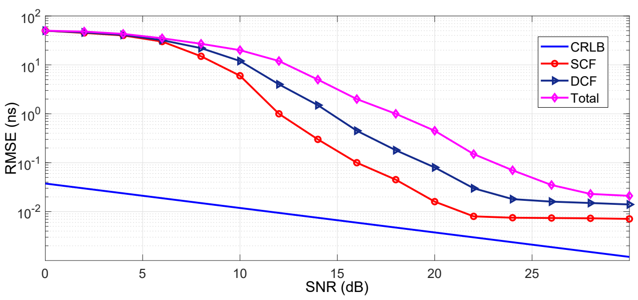

Fig. 8: RMSE vs. SRN for CFST method and CRLB.

3.2. Positioning Single Buried Object

Fig. 9 shows the result of determining the position of a single buried object using different types of pulses with the same parameter values listed in Tab. 1. To illustrate the graph more clearly, the units of Z_{ob} and d_{ob} in the figures are set to meters.

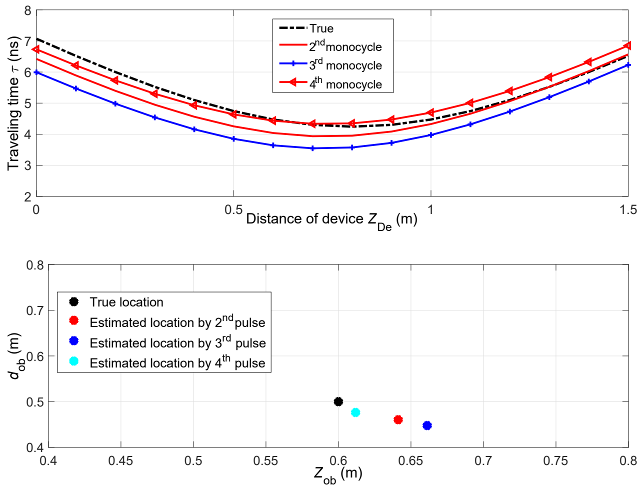

Fig. 9: The traveling time change according to the position of device (top) and the estimated positions of the single buried object (bottom).

The dashed black line denotes the traveling time according to the position of the device (see Eq. (4) and Eq. (9)) with the true values of the buried object $(Z_{\mathrm{ob}}, d_{\mathrm{ob}}, \varepsilon) = (60\ \mathrm{cm}, 50\ \mathrm{cm}, 4.5)$ and the remaining lines represent values estimated by the LMA with the 2^{nd}, 3^{rd} and 4^{th} order Gaussian monocycles. In addition, the true and estimated locations by the proposed method are indicated in Tab. 2, the positioning error using the 4^{th} order pulses in this scenario has an average value of about 2.4 cm, of the 2^{nd} order pulses is 4.5 cm, and of the 3^{rd} order pulses is 6 cm.

Tab. 2: The numerical results.

Notation	Z_{ob} (cm)	d_{ob} (cm)	ε
The true value	60	50	4.5
The estimated values with 2^{nd}-order Gaussian	64.12	46.05	4.2809
The estimated values with 3^{rd}-order Gaussian	66.12	44.77	4.1323
The estimated values with 4^{th}-order Gaussian	61.18	47.63	4.3266

One can observe that the performance using the 4^{th} order Gaussian monocycle is better than the others. This reason can be explained by comparing the auto-correlation functions of Gaussian monocycles as shown in Fig. 3. The shape of the auto-correlation function of the 3^{rd} order Gaussian monocycle has maximum points at $\tau = 0.32$ ns and $\tau = 0$ ns while the 2^{nd} and 4^{th} order Gaussian monocycles have only one extreme point at $\tau = 0$ ns. This leads to determining the traveling time using the correlation function of the third-order Gaussian monocycle with larger error than using other monocycles.

3.3. Positioning Adjacent Buried Objects

Based on the sample set of the correlation values in the case of positioning single buried object, the results of locating two adjacent objects is illustrated in Fig. 10 with the distance between them being 2 cm.

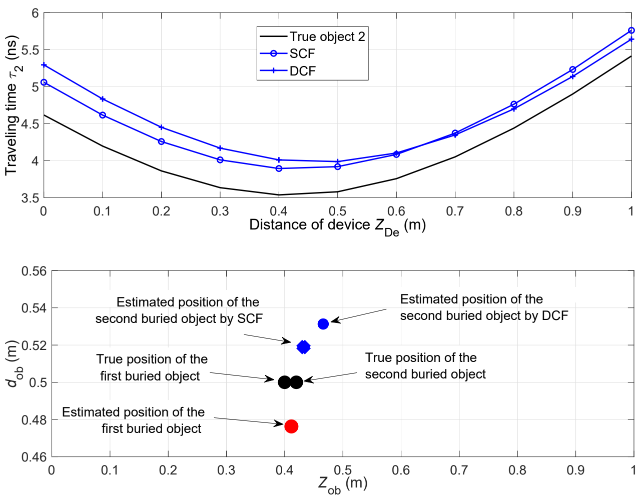

Fig. 10: Two adjacent buried objects: the traveling time change according to the device's translation (top) and the estimated position of the object by the CFST (bottom).

As seen in Fig. 10, the estimated error of using the SCF is smaller than using the DCF. The results can be explained by observing Fig. 6, Fig. 8, Eq. (19) (SCF) and Eq. (20) (DCF), we can see that the error of estimating traveling time parameter depends on the values of the correlation function, SNR and these values are proportional to the amplitude of received signal, hence the estimation error depends on the amplitude of received signal. Moreover, comparing the SCF and the DCF, we observe that in DCF, the amplitude of the reflected signal from the second object is reduced by the the division of the correlation functions. Hence, the value of the correlation function of the DCF also reduces, causing higher errors when determining traveling time rather than using the SCF.

Fig. 11 indicates the results of the CFST with three buried objects in the homogeneous environment. The position of the first buried object and the relative permittivity of the environment are determined at first, then, the location of the second, and the third object is located by CFST. If there are more buried objects, each next object will be located in turn, as the way to determine these three buried objects. In addition, Tab. 3 shows the comparison of the proposed method with conventional methods as reported in [6] and [7]. We observe that the proposed method improves the accuracy of locating the buried object with the average distance error achieved about 3.52 cm. The reason can be explained - the methods based on processing

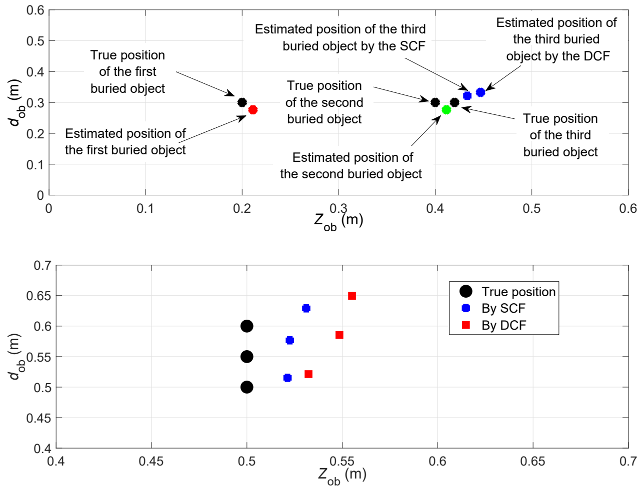

Fig. 11: The true and estimated locations by CFST method.

GPR images (Multiresolution Monogenic Signal Analysis, Wide-band chaotic) are indistinguishable the adjacent and tangent hyperbolas, and greatly affected by background noise. Meanwhile, the CFST can be used to solve this problem. With the ability to separate the adjacent hyperbolas, the performance of CFST is better than in the conventional method.

Tab. 3: The comparison of different methods.

Method	Distance error (cm)
The Multiresolution Monogenic Signal Analysis [6]	5.8
Wideband chaotic [7]	10
CFST	3.52

4. Conclusions

In this paper, we propose a method to locate multi-buried objects, especially adjacent objects based on analysis of correlation function and LMA for IR-UWB penetrating systems, called CFST. Our analysis indicates that, by processing the values of the correlation function between the reflected and template signals, we can determine the characteristics of the environment and the location of buried objects. The proposed method can be applied to locate the single buried object and adjacent buried objects. The performance of the IR-UWB system is assessed based on positioning errors and the CRLB of the TOA method. These errors depends on the order of Gaussian monocycles and the method analyze correlation function. Hence, the selection of the order of Gaussian monocycles and the correlation function analysis method depends on the specific application.

Author Contributions

H.N. and H.D. developed the theoretical about UWB signal and correlation function processing, performed analytical calculations and simulations on Matlab. All authors contributed to the final version of the manuscript. H.P. supervises the entire content of the article.

References

[1] FAN, X., F. WANG, W. GONG, L. ZHANG and J. LIU. Multiple Object Activity Identification Using RFIDs: A Multipath-Aware Deep Learning Solution. In: *2018 IEEE 38th International Conference on Distributed Computing Systems (ICDCS)*. Vienna: IEEE, 2018, pp. 545–555. ISBN 978-1-5386-6871-9. DOI: 10.1109/ICDCS.2018.00060.

[2] YAN, J., D. LIN, K. TANG, G. YANG and Q. YE. High Precision Indoor Positioning Method Based on UWB. In: *International Conference on Ad Hoc Networks ADHOCNETS 2019: Ad Hoc Networks*. Queenstown: Springer, 2019, pp. 201–207. ISBN 978-3-030-37262-0. DOI: 10.1007/978-3-030-37262-0_16.

[3] PARK, B., J. KIM, J. LEE, M.-S. KANG and Y.-K. AN. Underground Object Classification for Urban Roads Using Instantaneous Phase Analysis of Ground-Penetrating Radar (GPR) Data. *Remote Sensing*. 2018, vol. 10, iss. 9, pp. 1–23. ISSN 2072-4292. DOI: 10.3390/rs10091417.

[4] SALUCCI, M., L. TENUTI, L. POLI and A. MASSA. Buried object detection and imaging through innovative processing of GPR data. In: *2017 11th European Conference on Antennas and Propagation (EUCAP)*. Paris: AEEE, 2017, pp. 1703–1706. ISBN 978-8-8907-0187-0. DOI: 10.23919/EuCAP.2017.7928232.

[5] WANG, J., L. SANG and B. LI. The Detection of Buried Objects in Shallow Sea with Low Frequency Electromagnetic Waves. In: *2018 OCEANS - MTS/IEEE Kobe Techno-Oceans (OTO)*. Kobe: IEEE, 2018, pp. 1–6. ISBN 978-1-5386-1654-3. DOI: 10.1109/OCEANSKOBE.2018.8559390.

[6] QIAO, L., Y. QIN, X. REN and Q. WANG. Identification of Buried Objects in GPR Using Amplitude Modulated Signals Extracted from Multiresolution Monogenic Signal Analysis. *Sensors*. 2015, vol. 15, iss. 12, pp. 30340–30350. ISSN 1424-8220. DOI: 10.3390/s151229801.

[7] LI, J., T. GUO, H. LEUNG, H. XU, L. LIU, B. WANG and Y. LIU. Locating Underground Pipe Using Wideband Chaotic Ground Penetrating Radar. *Sensors*. 2019, vol. 19, iss. 13, pp. 1–12. ISSN 1424-8220. DOI: 10.3390/s19132913.

[8] ZHOU, X., H. CHEN and T. HAO. Efficient Detection of Buried Plastic Pipes by Combining GPR and Electric Field Methods. *IEEE Transactions on Geoscience and Remote Sensing*. 2019, vol. 57, iss. 6, pp. 3967–3979. ISSN 1558-0644. DOI: 10.1109/TGRS.2018.2889248.

[9] GUZEL, Y., M. A. ALPER, I. OZTURK and A. NASSIB. Imaging and analyzing a target buried in a two different inhomogeneous lossy medium. In: *2017 IEEE International Conference on Power, Control, Signals and Instrumentation Engineering (ICPCSI)*. Chennai: IEEE, 2017, pp. 152–156. ISBN 978-1-5386-0814-2. DOI: 10.1109/ICPCSI.2017.8392003.

[10] LIU, Y., D. HABIBI, D. CHAI, X. WANG, H. CHEN, Y. GAO and S. LI. A Comprehensive Review of Acoustic Methods for Locating Underground Pipelines. *Applied Sciences*. 2020, vol. 10, iss. 3, pp. 1–30. ISSN 2076-3417. DOI: 10.3390/app10031031.

[11] SANTOS, E. R. S., H. AZPURUA, P. A. F. REZECK, M. F. S. CORREA, M. A. M. VIEIRA, G. M. FREITAS and D. G. MACHARET. Localization Using Ultra Wideband and IEEE 802.15.4 Radios with Nonlinear Bayesian Filters: a Comparative Study. *Journal of Intelligent & Robotic Systems*. 2020, vol. 99, iss. 3, pp. 571–587. ISSN 1573-0409. DOI: 10.1007/s10846-019-01126-7.

[12] BHARADWAJ, R., S. SWAISAENYAKORN, C. G. PARINI, J. C. BATCHELOR and A. ALOMAINY. Impulse Radio Ultra-Wideband Communications for Localization and Tracking of Human Body and Limbs Movement for Healthcare Applications. *IEEE Transactions on Antennas and Propagation*. 2017, vol. 65, iss. 12, pp. 7298–7309. ISSN 1558-2221. DOI: 10.1109/TAP.2017.2759841.

[13] HUYEN, N. T. and P. T. HIEP. Proposing adaptive PN sequence length scheme for testing non-destructive structure using DS-UWB. In: *2019 3rd International Conference on Recent Advances in Signal Processing, Telecommunications & Computing (SigTelCom)*. Hanoi: IEEE, 2019, pp. 10–14. ISBN 978-1-5386-7963-0. DOI: 10.1109/SIGTELCOM.2019.8696169.

[14] BLANCO-MURILLO, J. L., D. LLUVERAS, V. Y. JIMENEZ, J. J. ANAYA, F. J. CASAJUS-

QUIROS, M. A. G. IZQUIERDO, J. M. MENENDEZ, M. G. HERNANDEZ and A. HERRERA. Combined US and UWB-RF imaging of concrete structures for identification and location of embedded materials. *Construction and Building Materials*. 2017, vol. 152, iss. 1, pp. 693–701. ISSN 1879-0526. DOI: 10.1016/j.conbuildmat.2017.07.036.

[15] KANZOW, C., N. YAMASHITA and M. FUKUSHIMA. WITHDRAWN: Levenberg–Marquardt methods with strong local convergence properties for solving nonlinear equations with convex constraints. *Journal of Computational and Applied Mathematics*. 2005, vol. 173, iss. 2, pp. 321–343. ISSN 1879-1778. DOI: 10.1016/j.cam.2004.03.015.

[16] SAHINOGLU, Z., S. GEZICI and I. GUVENC. *Ultra-wideband Positioning Systems: Theoretical Limits, Ranging Algorithms, and Protocols*. 1st ed. Cambridge: Cambridge University Press, 2008. ISBN 978-0-521-87309-3.

[17] CHEN, X. and S. KIAEI. Monocycle shapes for ultra wideband system. In: *2002 IEEE International Symposium on Circuits and Systems (ISCAS)*. Phoenix-Scottsdale: IEEE, 2002, pp. 597–600. ISBN 0-7803-7448-7. DOI: 10.1109/ISCAS.2002.1009911.

[18] GOTTLIEB, I. M. *Practical RF Power Design Techniques*. 1st ed. New York: McGraw-Hill/TAB Electronics, 1993. ISBN 978-0-8306-4129-1.

[19] LEE, S. H., S. M. IM, and I. S. HWANG. Quartic functional equations. *Journal of Mathematical Analysis and Applications*. 2005, vol. 307, iss. 2, pp. 387–394. ISSN 1096-0813. DOI: 10.1016/j.jmaa.2004.12.062.

[20] SOGANCI, H., S. GEZICI and H. V. POOR. Accurate positioning in ultra-wideband systems. *IEEE Wireless Communications*. 2011, vol. 18, iss. 2, pp. 19–27. ISSN 1558-0687. DOI: 10.1109/MWC.2011.5751292.

[21] HU, B. and N. C. BEAULIEU. Accurate evaluation of multiple-access performance in TH-PPM and TH-BPSK UWB systems. *IEEE Transactions on Communications*. 2004, vol. 52, iss. 10, pp. 1758–1766. ISSN 1558-0857. DOI: 10.1109/TCOMM.2004.836424.

About Authors

Huyen NGUYEN was born in Ha Noi City, Vietnam. She received the M.Sc. degree in electronic technical from Le Quy Don Technical University, in 2015. Her research interests include UWB radio in positioning, adaptive signal processing and measurement.

Ha DUONG was born in Ha Noi City, Vietnam. He received Ph.D. degree in Electrical Engineering from Moscow Aviation Institute, Russian Federation, in 2014. His research interests lie in the area of wireless information, UWB technology, adaptive signal processing and measurement.

Hiep PHAM (corresponding author) was born in Ha Noi City, Vietnam. He received the M.E. and Ph.D. degree in Physics, Electrical and Computer Engineering from Yokohama National University, Japan, in 2009 and 2012, respectively. His research interests lie in the area of wireless information, communications technologies, and Ultra Wide Band (UWB) radio in positioning, testing non-destructive structure by radio waves.